Collision and rebounding of circular rings on rigid target

Xu, Shanqing; Ruan, Dong; Lu, Guoxing; Yu, T.X.

2014

Xu, S., Ruan, D., Lu, G., & Yu, T. (2014). Collision and rebounding of circular rings on rigid target. International journal of impact engineering, in press.

https://hdl.handle.net/10356/101508

https://doi.org/10.1016/j.ijimpeng.2014.07.005

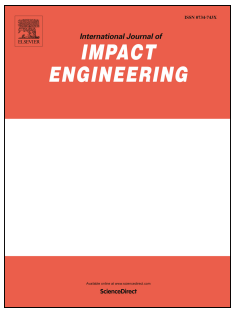

Collision and Rebounding of Circular Rings on Rigid Target

Shanqing Xu, Dong Ruan, Guoxing Lu, T.X. Yu

PII: S0734-743X(14)00151-1

DOI: 10.1016/j.ijimpeng.2014.07.005

Reference: IE 2372

To appear in: *International Journal of Impact Engineering*

Received Date: 5 January 2014

Revised Date: 12 June 2014

Accepted Date: 2 July 2014

Please cite this article as: Xu S, Ruan D, Lu G, Yu TX, Collision and Rebounding of Circular Rings on Rigid Target, *International Journal of Impact Engineering* (2014), doi: 10.1016/j.ijimpeng.2014.07.005.

Highlights

A specially designed testing technique was effectively applied to study the lateral impact behaviour of flying aluminium rings on a rigid target.

The influence of initial velocity and non-dimensional thickness of rings on the magnitude of peak force, the collision duration and the rebounding velocity was systematically investigated by experiments.

The dynamic deformation mechanism of flying rings to impact on a rigid target was analysed and its dependence on the initial impact velocity was discussed.

Collision and Rebounding of Circular Rings on Rigid Target

Shanqing Xu[a], Dong Ruan [a,1], Guoxing Lu[b] and T.X. Yu[c,d]

[a] *Faculty of Science, Engineering and Technology, Swinburne University of Technology, Hawthorn, Australia*
[b] *School of Mechanical and Aerospace Engineering, Nanyang Technological University, Singapore*
[c] *Department of Mechanical and Aerospace Engineering, Hong Kong University of Science and Technology, Clear Water Bay, Kowloon, Hong Kong*
[d] *Department of Engineering Mechanics, Zhejiang University, Hangzhou, Zhejiang, P.R. China*

Abstract

The collision behaviour of three types of circular aluminium rings was experimentally studied in this paper. A specially designed fixture attached to the barrel of an air gun was employed for the lateral impact of flying rings on a rigid target. The force history, deformation mechanisms and rebounding velocity of the rings, as well as their dependence on the wall thickness of rings and initial impact velocity were extensively investigated. The results showed that larger initial velocity and greater non-dimensional thickness led to larger magnitude of peak force. With the increase of initial velocity, the rebounding velocity first increased to a maximum value and then dropped, while the coefficient of restitution first decreased almost linearly and then leveled off at a lower level. However, the wall thickness of the ring only has a limited influence on both the rebounding velocity and the coefficient of restitution within the studied range. A six-hinge deformation mechanism was identified based on the four-phase deformation mode of the ring during its collision, which was captured in high speed camera recordings. Furthermore, it was observed that the impact force history was highly related to the deformation mode.

Keywords: Circular ring, Collision, Rebounding, Large deformation mechanism.

[1] Corresponding author. Faculty of Engineering and Industrial Sciences, Swinburne University of Technology, John Street, Hawthorn, VIC 3122, Australia. Tel.: +61 3 9214 8258, Email address: druan@swin.edu.au

1. Introduction

As a simple structural element, circular ring has attracted considerable attention in applied mechanics. Circular rings are widely used in energy absorbing system when impact occurs as they dissipate most kinetic energy by plastic deformation [1].

Numerous experimental and theoretical studies on quasi-static and dynamic compression of circular rings or ring systems between two rigid plates have been conducted [2-16], with a focus on the plastic deformation mechanisms. In 1963, DeRuntz and Hodge [2] pioneered a study on the quasi-static compression of thin-walled cylindrical tubes between two rigid plates. They first proposed an analytical model for rigid, perfectly plastic rings, assuming that the collapse mode consisted of four plastic hinges, which remained stationary relative to the rigid portions of the tube during the large deformation process. Separation occurred from the outset between the tube and the plates in the central portion of the contact zone. Burton and Craig [3] proposed an alternative model in which the tube was flattened in the contact zones and conformed to the shape of the plates throughout the loading. This model consisted of six hinges, four in the flattened contact zones and two in the parallel middle plane. Reid and Reddy [4] discussed the above two models and improved on DeRuntz and Hodge model by considering the strain-hardening effect. They argued that the neglect of strain-hardening could lead to substantial errors when the mode of deformation consisted principally of bending and no in-plane forces were developed or where their effects were minimal. Yu [5] also studied a rigid-plastic circular ring pulled by a pair of diametrically opposite point loads. The above mentioned analytical models are for quasi-static, large deformation of the rings.

Limited study can be found in literature on the dynamic behaviour of single rings under impact loading. The rigid, plastic deformation mechanism of a free ring under

concentrated dynamic loading was first studied by Owens and Symonds [6], and further analyzed by Hashmi et al [7]. Later, Shim et al. [8] experimentally studied the elastic wave propagation in dynamic compression of a single ring through a drop weight test, but only the wave propagation velocity was measured and no discussion was made on the deformation patterns.

Despite the limited open reports on the impact behaviour of single circular rings, Reid and co-workers [9-12] conducted a series of experimental and analytical studies on the impact behaviour of a chain of metal rings by using drop weight and sledge apparatus. They aimed at understanding the inertia effect when the ring systems were subjected to end impact and examination of a plastic shock model. In their study, a chain of rings (with and without plates between neighboring rings) with fixed end [9] and free end [11] was compressed by a sledge at velocities ranging from 30 to 120 m/s. They observed apparent wave-like phenomenon through the deformed rings and concluded that the deformation of the ring system was significantly affected by the propagation of structural shock wave. Based on the experimental observations, they proposed a structural shock theory [10] and pointed out that energy absorption was mainly attributed to the plastic deformation. The load-deflection curves obtained from the experiments and analytical model were in a good agreement. The model was updated after considering the effect of elastic deformation [12]. Liu et al. [13] also conducted an experimental and numerical study on the impact behaviour of a chain of rings. A modified split Hopkinson pressure bar was employed to study the propagation of stress waves. Deformation mechanisms of rings were not discussed, however. Most recently, Fan et al. [14] studied the dynamic lateral crushing of empty and sandwiched tubes by using a high speed Instron machine at 10 m/s. They did not observe significant difference in the collapse mode between the quasi-static and dynamic compression under loading velocities up to 10 m/s. However, their finite element analysis showed that the collapse mode would be

different when the velocity was beyond approximately 50 m/s.

Most studies on the crushing of circular rings have focused on the deformation patterns since they have great influence on the energy dissipation, with the interest in the crushing of either a ring compressed between two parallel rigid plates, or a ring (or a ring system) impinged by a rigid mass. A third loading scenario, i.e. a moving ring colliding on a rigid target along its lateral direction, has still not been investigated.

In this paper, the dynamic behaviour of a ring impacts onto a rigid anvil is studied experimentally. Ring specimens were fired out from the barrel of a split Hopkinson pressure bar (SHPB) onto a rigid target. The deformation patterns of 46 circular rings with three dimensions were experimentally characterized by using a high speed camera. The impact force-time history, the rebounding velocity (V_r) and coefficient of restitution are studied in relation to the initial impact velocity, as well as the ratio of the wall thickness (h) to the outer radius (R) of the ring.

2. Experiments

2.1. Materials and specimens

Aluminium rings of three dimensions (rings I, II and III) made of aluminium alloy 6061-T6 were tested. The rings were cut from commercial aluminium tubes. The nominal outer diameter and wall thickness of the three types of ring (R, h) were 28.5 mm, 0.91 mm; 25.4 mm, 0.91 mm; and 25.4 mm, 1.28 mm, respectively. The nominal width of all the ring specimens was 9.1 mm. The corresponding non-dimensional wall thicknesses, defined as the ratio of wall thickness to the outer radius ($\eta=h/R$), of the three types of specimens were 0.064, 0.072 and 0.1, respectively. Details of all the specimens are listed in Table 1. The tensile yield strength for aluminium alloy 6061-T6 was characterised on an MTS machine according

to ASTM E8M-08 test standard, with the test coupon cut from the same parent aluminium alloy tubes as for the rings. The gauge length was 50 mm. Two velocities for tension, 0.05 mm/s and 5 mm/s, were applied. The true stress versus the true strain curves were plotted in Fig. 1. The yield strength was found to be between 299 MPa and 305 MPa with an average value of 302 MPa. The Young's modulus was determined as 70 GPa. To assist identifying the deformation mechanism of the rings, red points were marked on one face of the ring with a spacing of 15 degrees circumferentially (Fig. 2a). It should be mentioned that due to the unavailability of rings with thicker walls (the diameter of the rings has to be fitted into the testing equipment), the study of the influence of thicker walls on the impact behaviour of rings will be conducted elsewhere through numerical simulation.

2.2. Equipment and test setup

Figure 2 shows the equipment and test arrangement of this study. To achieve a direct lateral impact of a ring on a rigid target, a novel insertion assembly was made. A rectangular-shaped casing made of aluminium alloy plates (2 mm thick) was sandwiched between two wooden blocks, which were polished into curved shapes to match the inner circular-shaped gun barrel of the air gun used in our existing SHPB system (see enlarged view in Fig. 2). Since the gun barrel has an inside diameter of 37 mm, the dimension for the rectangular casing was 32 mm × 12 mm. To minimize the effect of air flow on the movement of the ring after it flied off the barrel, the insertion assembly was extended to a distance of approximately 50 mm from the rigid target. Furthermore, to prevent possible movement of the insertion assembly in the test, a stopper was fixed on the supporting I-beam of the SHPB system at a proper location and it firmly grasped the wood plates. The end of the other single Hopkinson bar was used as the rigid target. By adjusting the alignment of this Hopkinson bar the direction of the insertion assembly was set perpendicular to the target surface. As this long, cylindrical, aluminium alloy bar of 37 mm in diameter had much larger rigidity and mass compared with those of the

ring specimens, it could be considered as a rigid fixed target.

To pick up the strain signals during the collision, two sets of semi-conductive strain gauges with a gauge factor of 110 were mounted diametrically oppositely on the Hopkinson bar's cylindrical surface at a location of 250 mm away from the impact end and were connected to a strain amplifier through bridge boxes. The amplified strain signals were then recorded using a Tektronix 2024B oscilloscope with bandwidth of 200 MHz and sampling rate of 2 GS/s.

A high speed camera was placed near the exit of the barrel, facing the lateral plane of the ring specimen, in order to capture the collision event of the ring to the rigid target. During the collision, the camera was set to record images at a rate of 50,000 frames per second, which was sufficiently fast to capture the details of the ring's deformation. Theoretically speaking, the rebounding velocity of a ring should be the velocity at the mass center of the ring. The initial velocity of the mass center can be easily determined because all the points in the ring had the same velocity when the ring is about to touch the rigid target. However, it was practically difficult to determine either the displacement or the velocity of the mass centre of the ring after the collision, as there was no physical point at the mass centre whose motion could be captured by the high speed camera. Therefore, to determine the rebounding velocity, the velocity (in the impact direction) of each point marked on the ring (Fig. 2a) was calculated based on the measurement of the displacements of the points in the images from the high speed camera. The average velocity of these velocities represented the velocity at the mass centre, i.e., the rebounding velocity of the ring when the ring just departed from the rigid target. When calculating the rebounding velocity, the motion of each point on the ring was traced for duration of 0.6 ms (30 frames in the high speed camera images) after the ring departed from the rigid surface.

2.3. Measurement of impact force and data processing

In this study, the impact force was calculated by

$$F(t) = E_0 A_0 \varepsilon(t) \tag{1}$$

where E_0 and A_0 are the Young's modulus and cross-sectional area of the aluminium bar, E_0=70 GPa and A_0=1075.21 mm^2. Calculated from the strain signal $\varepsilon(t)$ recorded by the strain gauge and oscilloscope, a typical force history of a collision test is plotted in Fig. 3. It can be seen that in the early stage of the collision significant oscillations occurred. From an analysis of the test results using Fast Fourier Transform (FFT), high frequency components beyond 125 kHz have a negligible effect on the overall shape of the force-time curve. Thus, the signals were filtered with a cut-off frequency of 125 kHz, resulting in a filtered curve as also plotted in Fig. 3, which is much smoother and easier to analyse. Consequently, in this paper, the analyses related to force history are all based on the FFT smoothed curves.

3. Results and discussion

3.1. Force history

Figure 4 shows a typical history of the impact force for the three types of aluminium rings I, II and III. In general, after the first peak, the impact force gradually declines to a rather lower level. With the collision proceeding, the impact force then starts to plateau out. When the initial impact velocity is not very high (e.g. up to 78 m/s, as shown in Fig. 4a) and rings are not fully crushed, the impact force drops to zero when the ring detaches from the rigid target. However, when the impact velocity is high (e.g. 125 m/s in Fig. 4a), the deformation of the ring is so much that the remote side of the ring contacts the impact side at certain velocity, resulting in a second peak.

The magnitude of the peak force is dependent on the initial impact velocity and the

non-dimensional thickness (h/R) of rings. As shown in Fig. 5a, for Ring I (h/R=0.064, mass=1.9 g), the peak force increases from 0.7 kN at 23.8 m/s to 4.5 kN at 125 m/s. For Ring II (h/R=0.072, mass=1.7 g), it increases from 0.5 kN at 19.8m/s to 3.2 kN at 101.4 m/s, while for Ring III (h/R=0.1, mass=2.3g), it is from 1.1 kN at 17.2 m/s to 5.4 kN at 114.8 m/s. On the other hand, the peak force also increases with the increase of non-dimensional thickness, or mass if the diameter of the ring is identical. As it can be seen from Fig. 5a, at a fixed initial velocity, Ring III (h/R=0.1, mass=2.3g) has a much larger peak force than Rings I and II. This shows that the peak force is highly sensitive to the mass of rings.

The collision duration T, i.e. the time interval between the first contact and complete detachment, is also dependent on both the initial impact velocity (V_0) and h/R ratio, according to the experimental observations. With the increase of h/R ratio, the collision duration decreases. For example, at an initial impact velocity of approximately 60 m/s, the collision durations for Ring I (h/R=0.064), Ring II (h/R=0.072) and Ring III (h/R=0.1) are 0.47 ms, 0.37 ms and 0.27 ms, respectively. For each type of the rings, in general, with the increase of the initial impact velocity, the collision duration increases at low velocity range. However, when the velocity reaches a value that the ring could be fully crushed, the collision duration decreases with the increasing velocity. Figure 5b clearly shows this trend. The collision duration for Ring I increases from 0.31 ms at 23.8 m/s to approximately 0.45 ms at 56.5 to 78.2 m/s and then drops to 0.3 ms at 125 m/s, when the ring is fully crushed. This trend can also be seen in Ring II (Fig. 5). But for Ring III, when it is fully crushed the collision duration remains stable.

3.2. Rebounding velocity and coefficient of restitution

From a dimensional analysis, two non-dimensional parameters emerge, i.e., non-dimensional wall thickness, $\eta=h/R$, and non-dimensional impact velocity, $v_0= V_0/V_Y$, where $V_Y=Y/(E\rho)^{1/2}$

denotes the yield velocity of the ring material. The yield stress Y of aluminium alloy 6061-T6 is measured as between 299 to 305 MPa. Using Young's modulus E=70 GPa and density ρ=2760 kg/m^3, the yield velocity for this material is found as V_Y=21.5~21.9 m/s. Hence, an average value, V_Y=21.7 m/s, is employed in the following.

Figure 6 shows the relationship between the non-dimensional rebounding velocity ($v_r=V_r/V_Y$) and the non-dimensional impact velocity (v_0) for the three types of circular rings, with the values of the rebounding velocity listed in Table 1. It is evident that the rebounding velocity reaches a maximum value (approximately 0.6~0.7V_Y) when the impact velocity increases approximately 2~3 times the yield velocity, V_Y. After that, the rebounding velocity continuingly decreases with the increase of impact velocity, then later approaching a stable value around 0.3V_Y when the impact velocity is higher than 5~6 times of V_Y. In Fig. 6, the odd data points at approximately v_0=4.5 show rather low values. The reason is unclear, which requires further investigation. The non-dimensional wall thickness, $\eta=h/R$, only displays minor influence on the rebounding velocity within the studied range.

Figure 7 demonstrates the dependence of the coefficient of restitution (COR=v_r/v_0) on the initial impact velocity for the three types of circular rings. With the increase of the initial impact velocity from 1 to 4.5 times of the yield velocity, the coefficient of restitution decreases almost in a linear fashion from about 0.5 to 0.05 and then it plateaus at this level for higher velocities. Since the rebounding of the rings reflects the elastic energy stored in the ring, the extremely low level of COR at high impact velocity implies that a major share of the kinetic energy during the collision is dissipated in the plastic deformation. Furthermore, it is interesting to note that the coefficient of restitution is not significantly affected by the non-dimensional wall thickness, h/R.

3.3. Dynamic deformation mechanism

Figure 8 shows the final deformed shape of the rings after the collision tests. As seen in the figure, the non-dimensional wall thickness (h/R) has limited influence on the deformation pattern as no evident difference is observed. The final deformed shapes of the rings demonstrate two main common features. Firstly, at high velocities, both the collision side (Point A in Fig. 9) and the remote side (Point E in Fig. 9) of the ring become concave so as to form a V-like shape. The deformation occurs in the region adjacent to the central points of the two sides. Secondly, at high velocities, the curvature of the ring on both flanks of the ring (Points F and G in Fig. 9) is much larger than what appears at low velocities. If the input kinetic energy is not sufficiently high, the regions near F and G would not deform.

A comparison of the deformation history of collided rings under three typical velocities is depicted in Fig. 10. On one hand, at low velocities (V_0<40 m/s), no concave portions are observed at either the collision or remote side. With the increase of initial impact velocity, the collision side starts to become concave. At even higher velocities (V_0>60 m/s), both sides become concave. On the other hand, with the collision proceeding, the collision side flattens first to form a segment BB□ (Fig. 9) (Phase I) and then the central region around point A (the center of segment BB□, also the first impact point) starts to become concave (Phase II). In the meantime, segment BB□ keeps propagating to the neighboring region, e.g., to points C and C□. At this stage, points E, F and G remain almost stationary in relation to the center of the ring, i.e., the deformation of the remote half of the ring is rather moderate and likely to be within the elastic range. When segment BB□ becomes relatively stable, the edge neighboring to point E starts to yield and becomes flattened (Phase III), resulting in the commencement of notable deformation of the remote half ring. Given a sufficient initial velocity, the portion near point E would also become concave (Phase IV). Phases III and IV occur only when the initial velocity is higher than a certain value. As observed from the high speed camera recordings, Phase III occurs when V_0 is equal to 23.8 m/s, 31.2m/s and 39.5 m/s

(i.e., V_0=1.1V_Y, 1.4V_Y and 1.8V_Y) for Ring I, Ring II and Ring III, respectively, while Phase IV occurs when V_0=68.7 m/s, 72.7 m/s and 76.5 m/s (i.e., V_0=3.2V_Y, 3.4V_Y and 3.5V_Y) for Rings I, II and III, respectively. Based on the above observations, the dynamic deformation mechanisms of a circular ring can be analyzed by separating it into four segments, as shown in Fig. 9 for Phase II to IV, i.e., segments AF, AG, EF and EG. Therefore, at least four plastic hinges (B, B′, F and G) could be identified at low impact velocity, similar to the model proposed by DeRuntz and Hodge [2] for the quasi-static compression, or that by Owens and Symonds [6] for dynamic deformation. For example, no evident concave shape near points A and E was observed for those rings collided at V_0=48.3 m/s (Fig. 10a), 40.4 m/s (Fig. 10b) and 39.5 m/s (Fig. 10a). However, at higher impact velocity, e.g., when V_0=94.4 m/s (Fig. 10a), 93.5 m/s (Fig. 10b) and 91.8 m/s (Fig. 10a), the regions near points A and E were observed to be concave. Therefore, a complete collapse of ring would contain six hinges, i.e., A, B, B′, E, F and G. The deformation mode is a six-hinge mechanism. In the earlier stage of the collision (Phase I), only the flattened segment BB□ needs to be analyzed since the rest of the ring remains unchanged. A detailed analytical model based on these observations will be carried out in the near future. It should be mentioned that the two hinges, F and G, are observed to be the central points of the two flank sides, i.e., the collision and remote half rings are equal in length, although the deformed shape of the two sides is not mirror image.

To further analyze the relationship between the deformation and the impact force, the force history of a typical ring (h/R=0.072, Ring II) impinging at 72.7 m/s is plotted in Fig. 11, together with the images recorded by the high speed camera. The initial impact in Phase I results in a peak force, which is slightly ahead of point ① at 0.02 ms. In Phase II, the portion near contacting point A starts to become concave and the corresponding force gradually decreases (point ② at 0.04 ms). Before Phase III starts, the force keeps declining from points

② to ⑤, with the time from 0.04 ms to 0.1 ms. At approximately 0.12 ms, the edge adjacent to the central point of the remote side (E) starts to yield and becomes flattened (Phase III), resulting in a drop of impact force. From point ⑦ onward (t>0.12 ms), point E of the remote side starts to become concave and the corresponding force slightly increases first and then plateaus out. Before the detachment of the ring from the rigid target, the force decreases gradually since most of the kinetic energy has been dissipated in the plastic deformation of the ring.

4. Conclusion

The dynamic behaviour of three types of circular aluminium rings was experimentally studied by firing the rings to impact laterally onto a rigid target. The force history, deformation mechanisms and rebounding velocity of the rings, as well as their dependence on the non-dimensional (h/R) and initial impact velocity (V_0) were extensively investigated. The main findings are as follows.

The first peak force during the collision is dependent on the initial velocity and the non-dimensional thickness (h/R) of the ring; larger initial velocity and greater h/R lead to higher magnitude of peak force. The collision duration is also dependent on the initial velocity and the non-dimensional wall thickness $\eta=h/R$. With the increase of $\eta=h/R$, the collision duration always decreases. With the increase of the initial impact velocity, the collision duration increases at low velocities to a maximum value and then decreases when the remote side of the ring contacts the collision side at very high velocities.

When the non-dimensional velocity ($v_0= V_0/V_Y$) increases to 2~3, the non-dimensional rebounding velocity ($v_r=V_r/V_Y$) reaches a maximum value (approximately 0.6~0.7). It drops continuingly and later approaches a stable value. With the increase of the impact velocity, the

coefficient of restitution first decreases almost in a linear fashion, and then levels off at a rather low level. The non-dimensional thickness ($\eta=h/R$) has a limited influence on the rebounding velocity and the coefficient of restitution, for the parameters within the range studied.

Four-hinge or six-hinge deformation mechanisms were identified depending on the initial velocity. It has also been revealed that impact force history is highly related to the deformation mechanisms. An analytical model based on the experimental observations in this study will be proposed and studied later on.

Acknowledgements: The authors wish to thank the Australian Research Council for financial support through a Discovery Grant and Mr Gayan Rathnaweera for help with the tensile tests of the aluminium alloy employed in this study. The 3rd author (G. Lu) also acknowledges the support from the State Key Laboratory of Explosion Science and Technology (Beijing Institute of Technology) (project KFJJ13-2Z).

References

[1] A.A.A. Alghamdi, Collapsible impact energy absorbers: An overview, Thin-Walled Struct., 39 (2001) 189-213.

[2] J.J.A. DeRuntz, J.P.G. Hodge, Crushing of a Tube Between Rigid Plates, J. Appl. Mech., 30 (1963) 391-395.

[3] R. Burton, J. Craig, An investigation into the energy absorbing properties of metal tubes loaded in the transverse direction, BSc (Engg) Report, University of Bristol, England, (1963).

[4] S.R. Reid, T.Y. Reddy, Effect of strain hardening on the lateral compression of tubes between rigid plates, Int. J. Solid. and Struct., 14 (1978) 213-225.

[5] T.X. Yu, Large plastic deformation of a circular ring pulled diametrically, Acta Mech. Sinica, 11 (1979) 88-91.

[6] R.H. Owens and P.S. Symonds, Plastic deformation of free ring under concentrated dynamic loading, J. Appl. Mech., 22 (1955), 523-529.

[7] S.J. Hashmi, S.T.S. Al-Hassani and W. Johnson, Dynamic plastic deformation of rings under impulsive load, Int. J. Mech. Sci., 14 (1972), 823-841.

[8] V.P.W. Shim, R. Lan, Y.B. Guo, L.M. Yang, Elastic wave propagation in cellular systems-Experiments on single rings and ring systems, Int. J. Impact Eng., 34 (2007) 1565-1584.

[9] S.R. Reid, T.Y. Reddy, Experimental investigation of inertia effects in one-dimensional metal ring systems subjected to end impact — I. Fixed-ended systems, Int. J. Impact Eng., 1 (1983) 85-106.

[10] S.R. Reid, W.W. Bell, R.A. Barr, Structural plastic shock model for one-dimensional ring systems, Int. J. Impact Eng., 1 (1983) 175-191.

[11] T.Y. Reddy, S.R. Reid, R. Barr, Experimental investigation of inertia effects in one-dimensional metal ring systems subjected to end impact-II. Free-ended systems, Int. J. Impact Eng., 11 (1991) 463-480.

[12] S.R. Reid, W.W. Bell, Response of one-dimensional metal ring system to end impact, in: J. Harding (Ed.), Inst of Physics, Oxford, Engl, 1984, pp. 471-478.

[13] K. Liu, K. Zhao, Z. Gao, T.X. Yu, Dynamic behavior of ring systems subjected to pulse loading, Int. J. Impact Eng., 31 (2005) 1209-1222.

[14] Z. Fan, J. Shen, G. Lu, D. Ruan, Dynamic lateral crushing of empty and sandwich tubes, Int. J. Impact Eng., 53 (2013) 3-16.

[15] N.K. Gupta, H. Abbas, Lateral collapse of composite cylindrical tubes between flat platens, Int. J. Impact Eng., 24 (2000) 329-346.

[16] D.K. Leu, Finite-element simulation of the lateral compression of aluminium tube between rigid plates, Int. J. Mech. Sci., 41 (1999) 621-638.

[17] T. Yella Reddy, S.R. Reid, Lateral compression of tubes and tube-systems with side constraints, Int. J. Mech. Sci., 21 (1979) 187-199.

Figure Captions

Fig. 1. True stress vs. true strain curves of aluminium alloy 6061-T6 conducted on an MTS machine at 0.05 mm/s and 5 mm/s.

Fig. 2. Test set-up for ring collision: (a) a sketch of the testing set-up, and (b) a photograph of the testing equipment.

Fig. 3. Original force signals and filtered signals by cutting off higher frequencies (125 kHz and beyond).

Fig. 4. Force histories of circular rings at different impact velocities for (a) Ring I; (b) Ring II and (c) Ring III (m, h, R and η are the mass, wall thickness, outer radius and ratio of wall thickness to outer radius of a ring, respectively).

Fig. 5. Peak force, collision duration in relation to the initial velocity and the non-dimensional thickness of rings: (a) peak force vs. initial velocity and (b) collision duration vs. initial velocity.

Fig. 6. The rebounding velocity versus the initial velocity for circular rings, V_Y=21.7 m/s.

Fig. 7. The coefficient of restitution (COR) versus non-dimensional initial velocity for circular rings with various h/R ratios.

Fig. 8. Final deformed shape of circular rings after collision at various velocities.

Fig. 9. A sketch of a deformed circular ring showing the initial stage of the collision on a rigid target.

Fig. 10. Comparison of deformed shape of rings after collision at different initial velocities: (a) Ring I (h/R=0.064), (b) Ring II (h/R=0.072) and (c) Ring III (h/R=0.1).

Fig. 11. Deformation patterns at different time instants during collision at V_0=72.7 m/s and the corresponding force amplitude of a typical circular ring with non-dimensional thickness h/R=0.072.

Figure 1

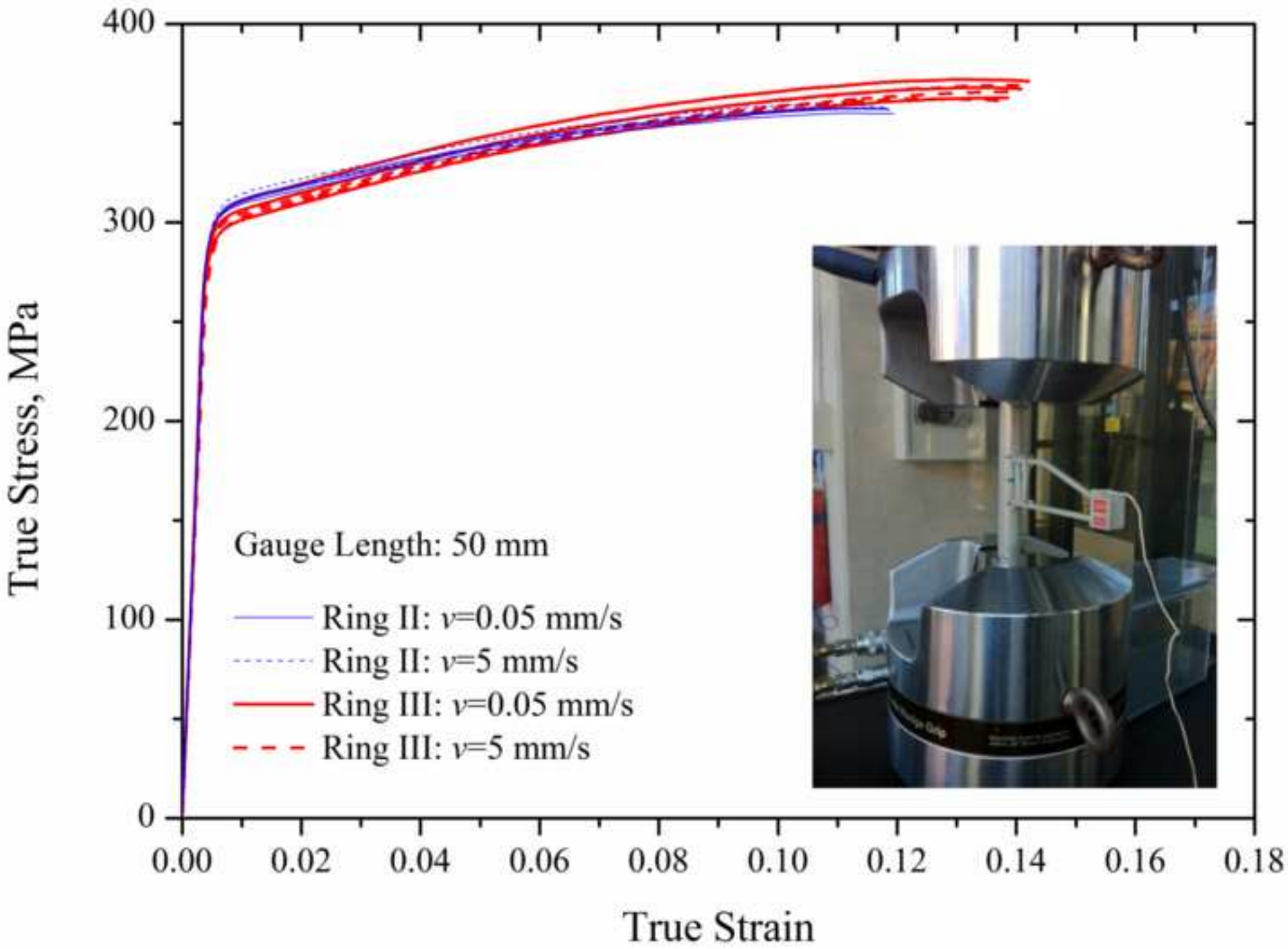

Figure 2

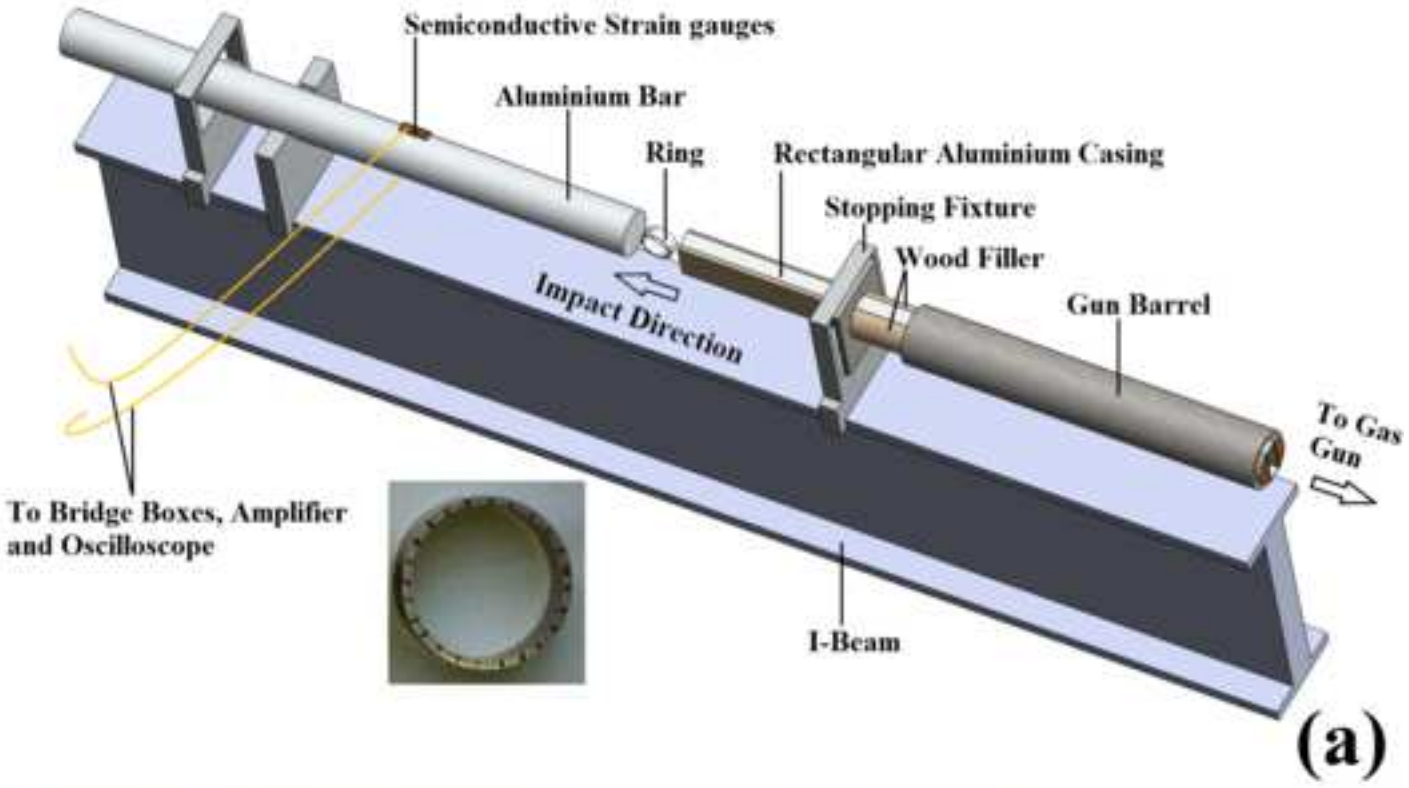
Semiconductive Strain gauges
Aluminium Bar
Ring
Rectangular Aluminium Casing
Stopping Fixture
Wood Filler
Gun Barrel
Impact Direction
To Gas Gun
To Bridge Boxes, Amplifier and Oscilloscope
I-Beam
(a)


Strain Gauge Bridge Box
Light
High Speed Camera
Amplifier
Oscilloscope
Stopper
(b)

Figure 3

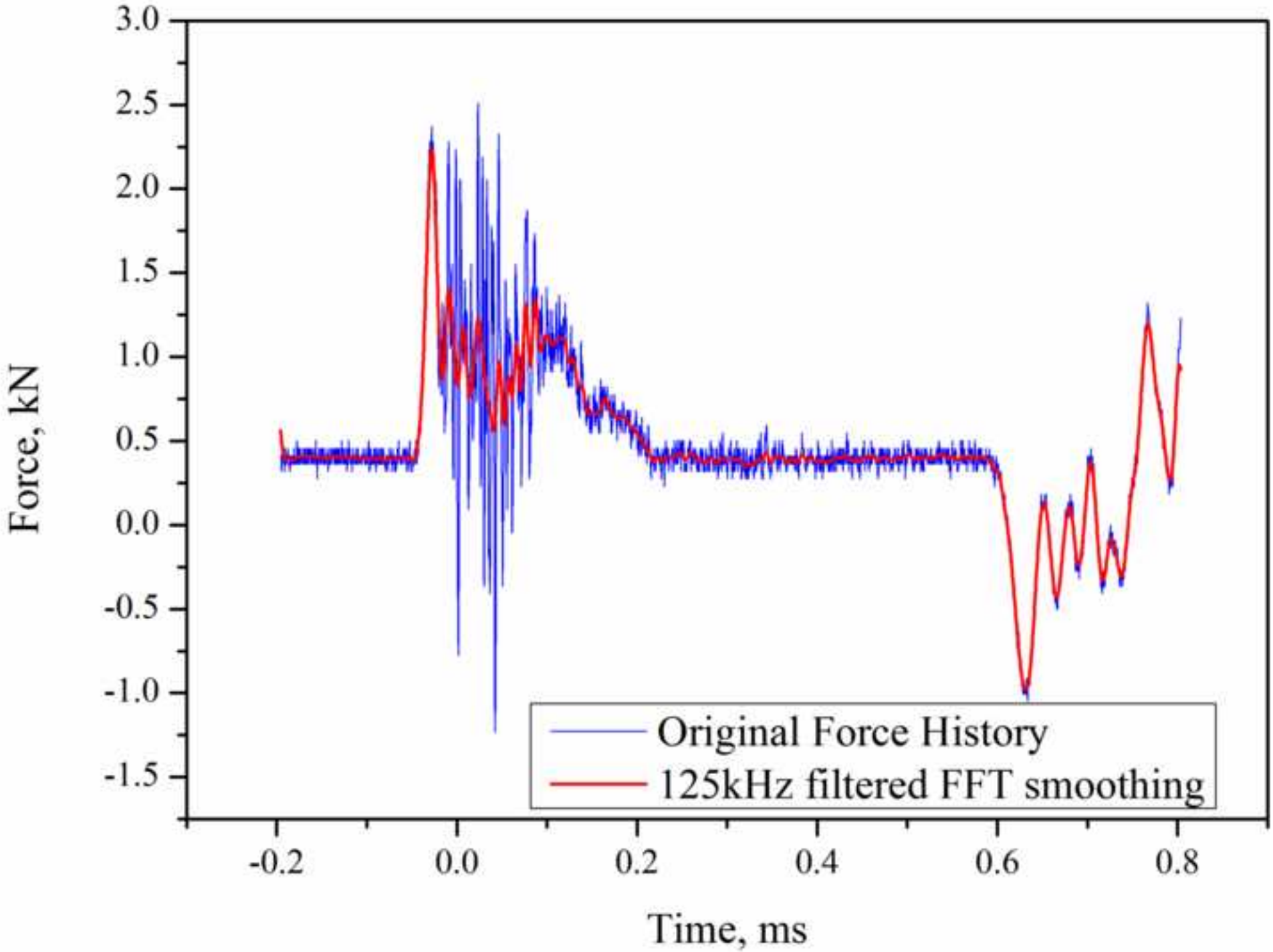

Figure 4

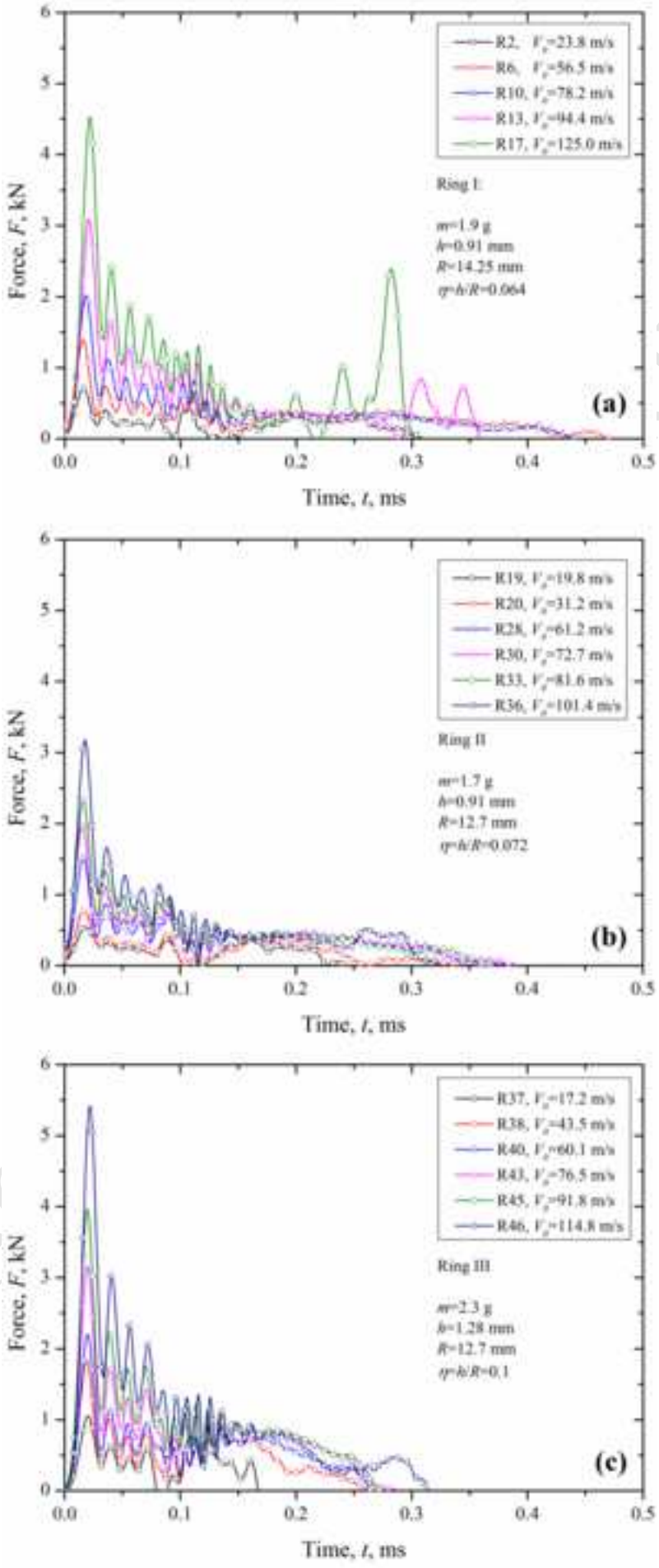

Figure 5

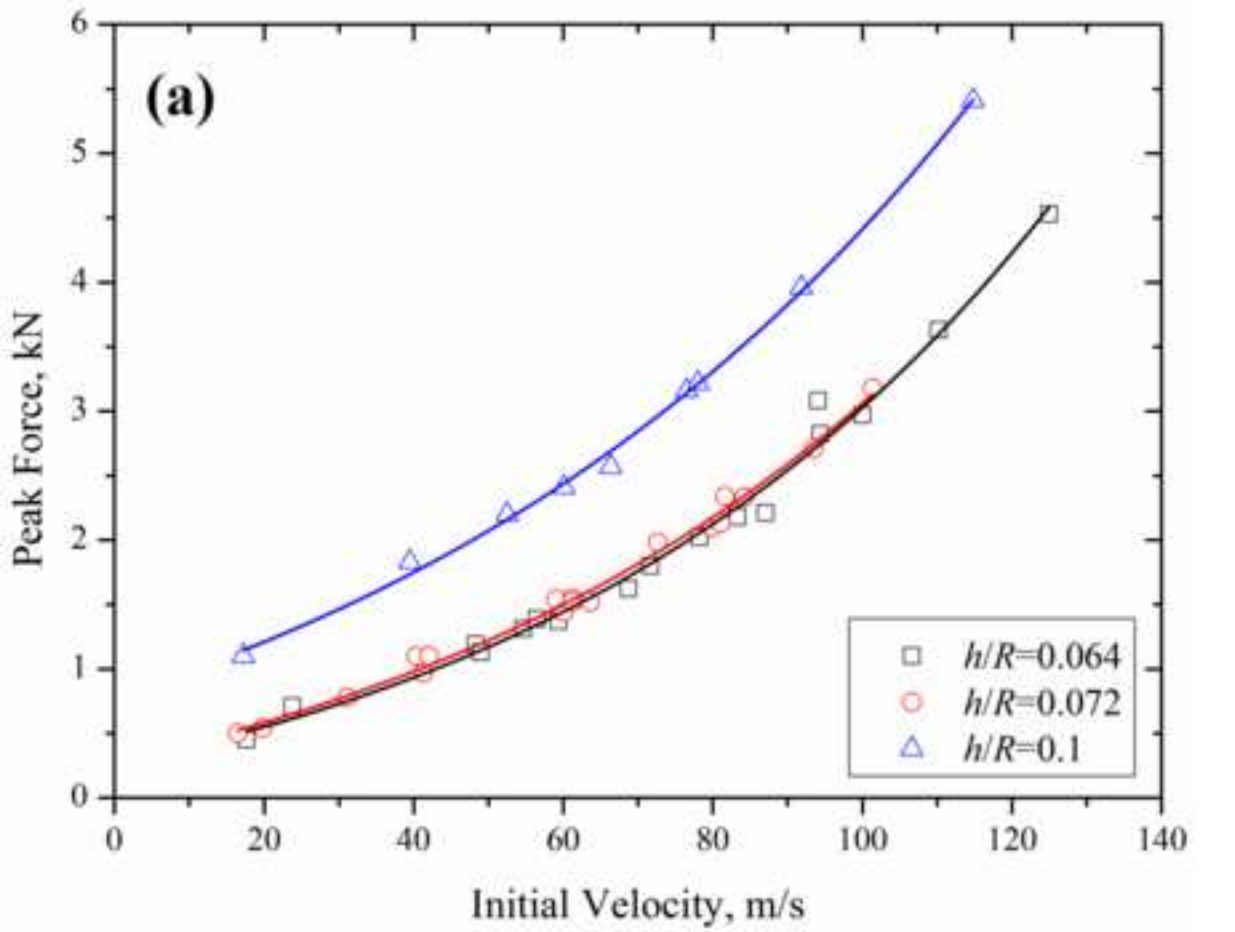
(a)
Peak Force, kN
Initial Velocity, m/s
h/R=0.064
h/R=0.072
h/R=0.1
0
1
2
3
4
5
6
0
20
40
60
80
100
120
140

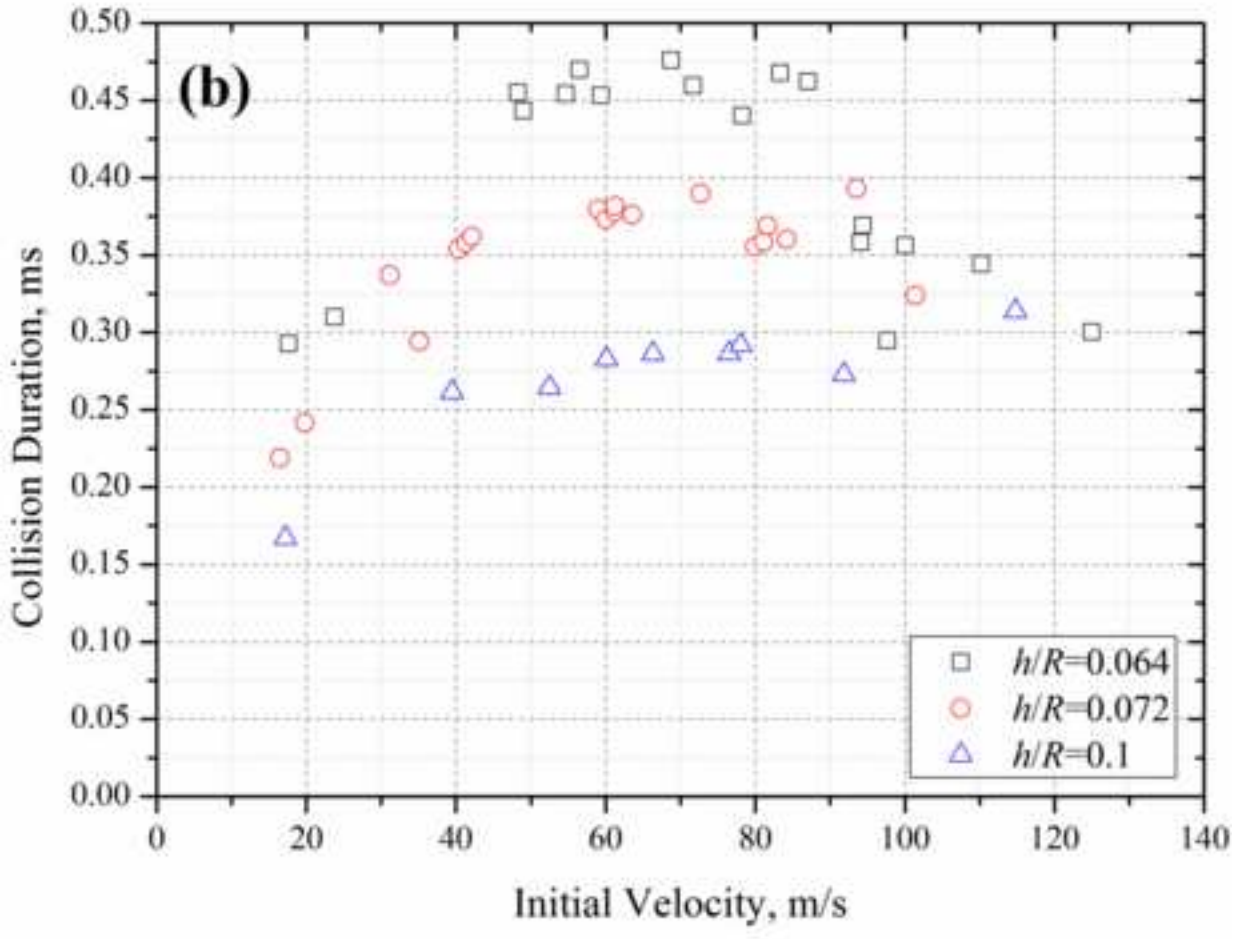
(b)
Collision Duration, ms
Initial Velocity, m/s
h/R=0.064
h/R=0.072
h/R=0.1
0.00
0.05
0.10
0.15
0.20
0.25
0.30
0.35
0.40
0.45
0.50
0
20
40
60
80
100
120
140

Figure 6

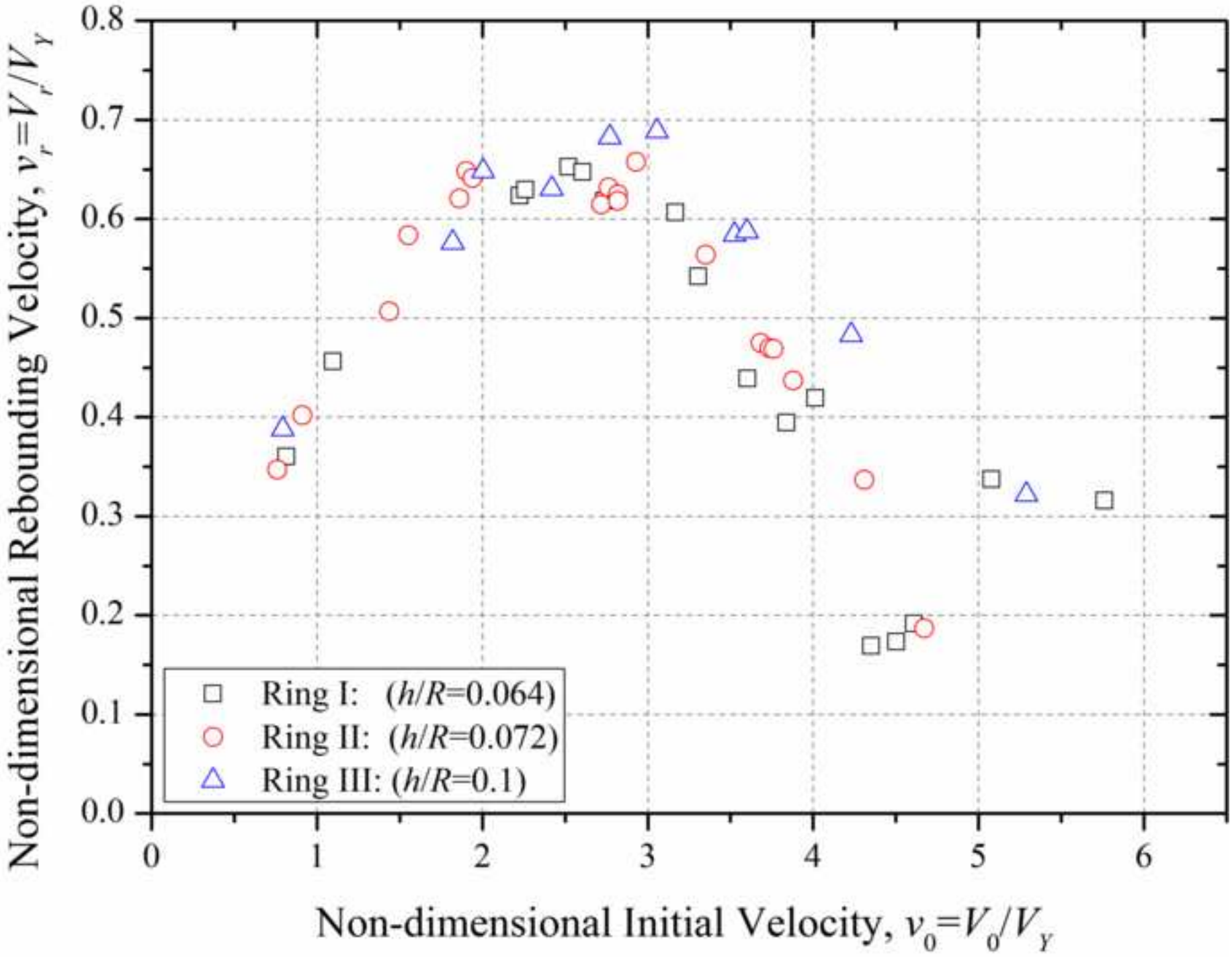

Figure 7

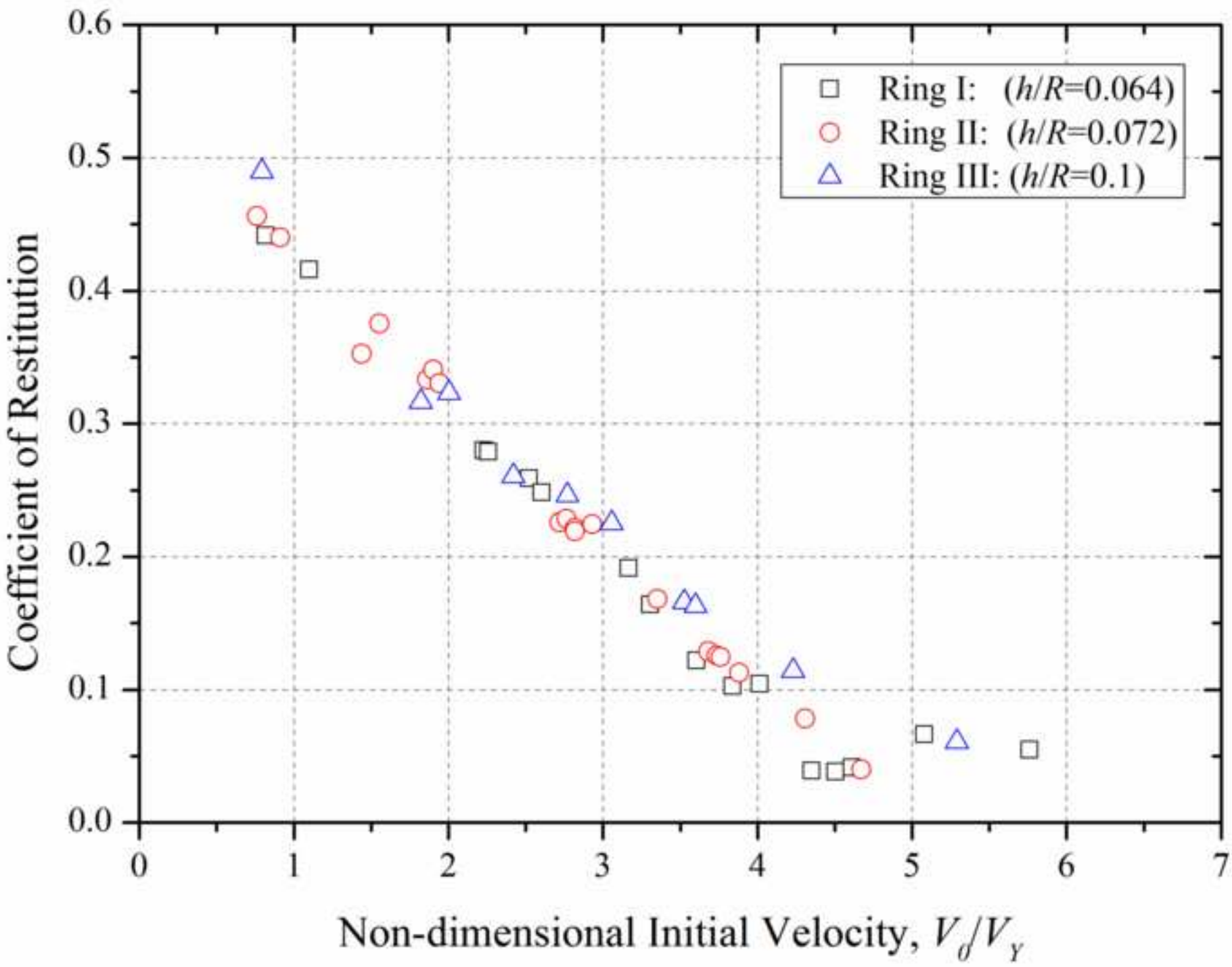

Figure 8

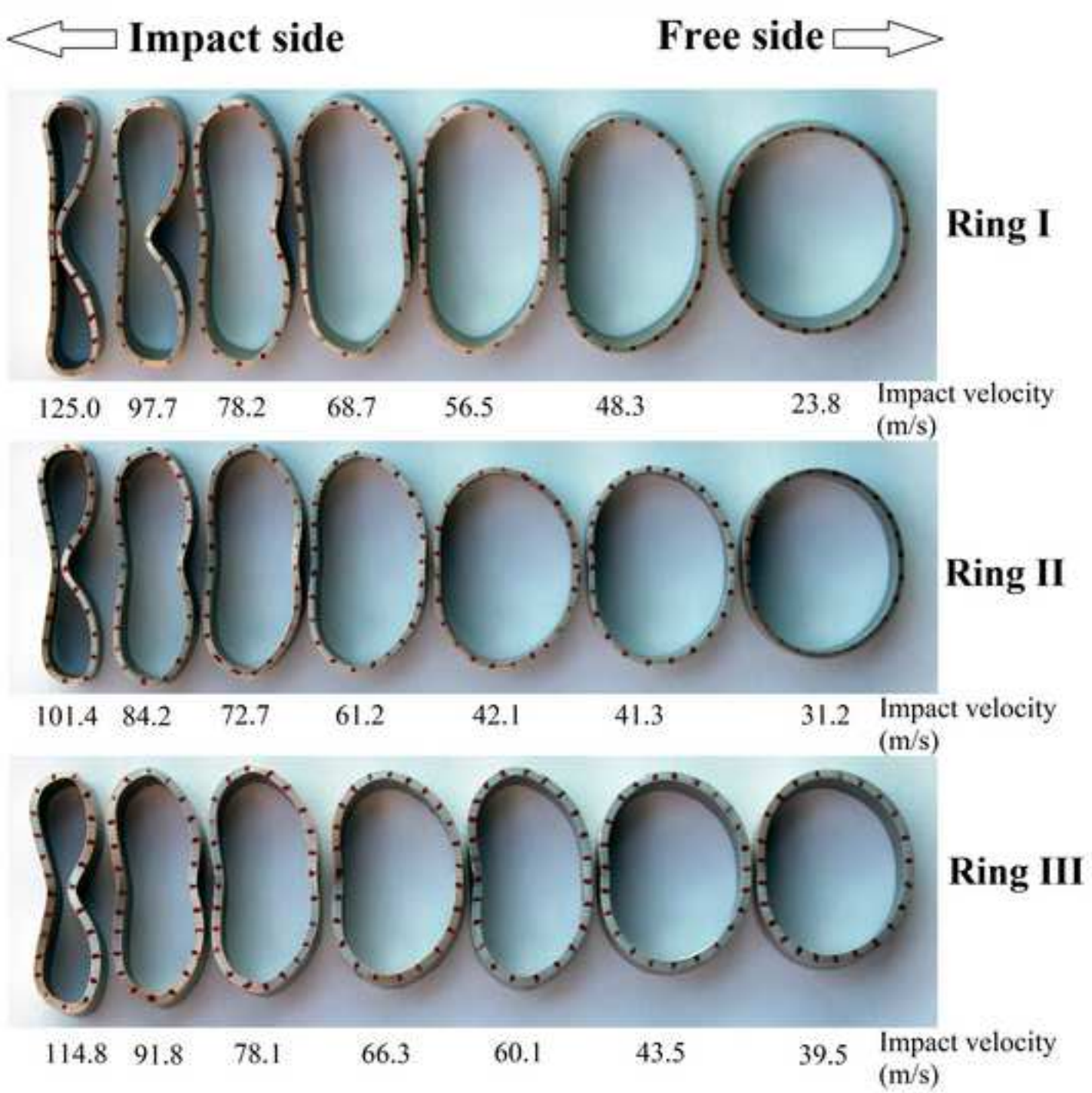

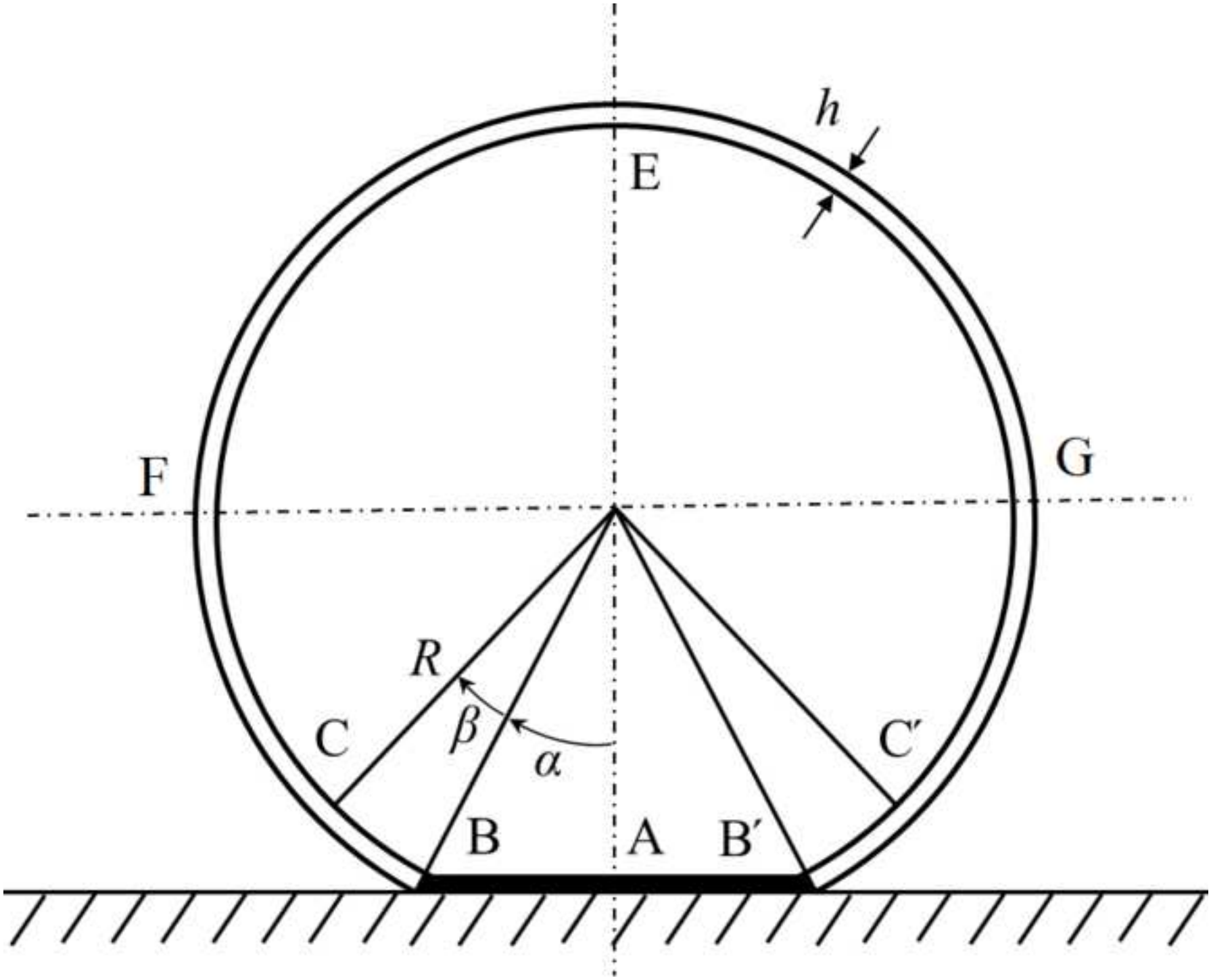

Figure 10

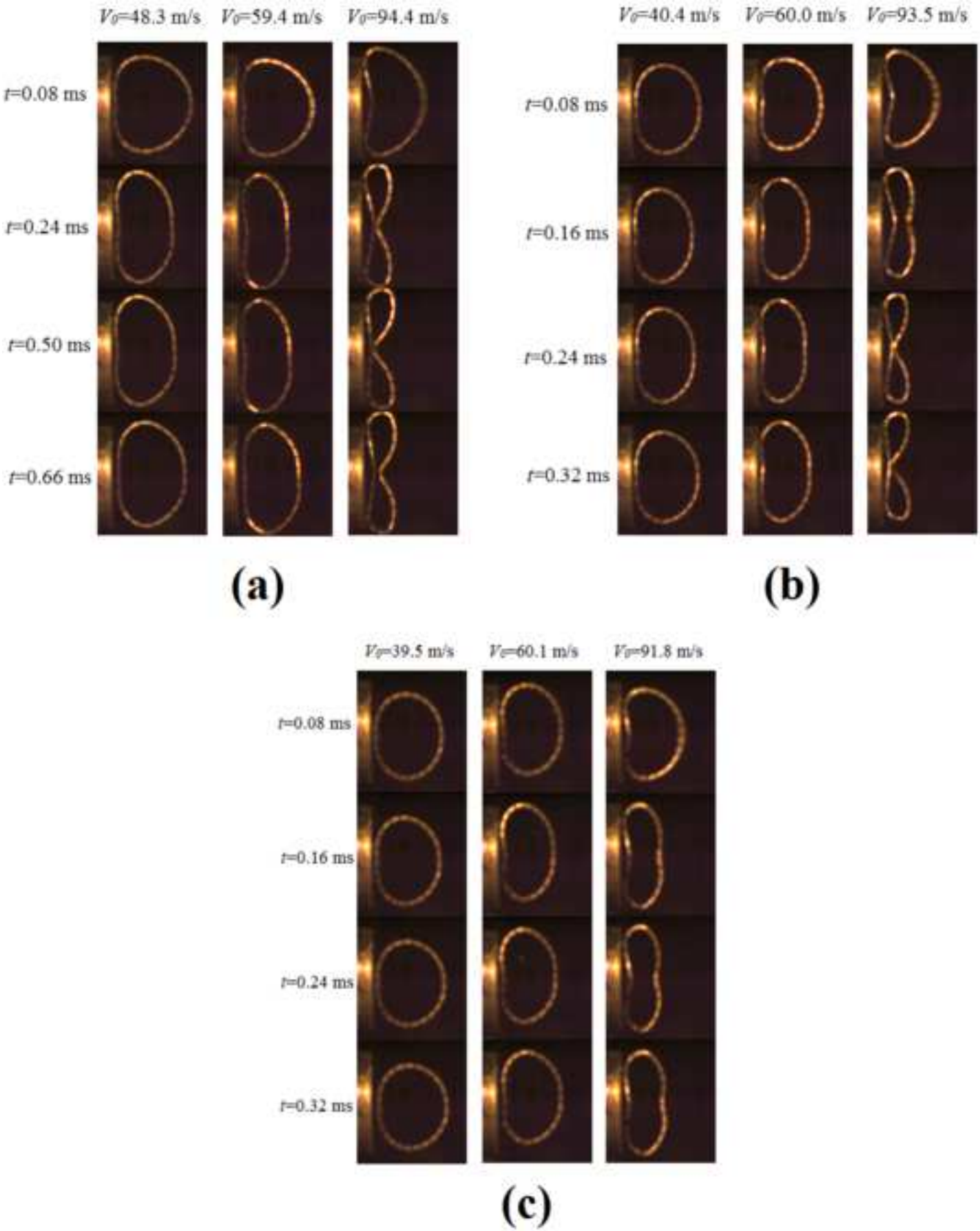
V_0=48.3 m/s
V_0=59.4 m/s
V_0=94.4 m/s
t=0.08 ms
t=0.24 ms
t=0.50 ms
t=0.66 ms
(a)
V_0=40.4 m/s
V_0=60.0 m/s
V_0=93.5 m/s
t=0.08 ms
t=0.16 ms
t=0.24 ms
t=0.32 ms
(b)
V_0=39.5 m/s
V_0=60.1 m/s
V_0=91.8 m/s
t=0.08 ms
t=0.16 ms
t=0.24 ms
t=0.32 ms
(c)

Figure 11

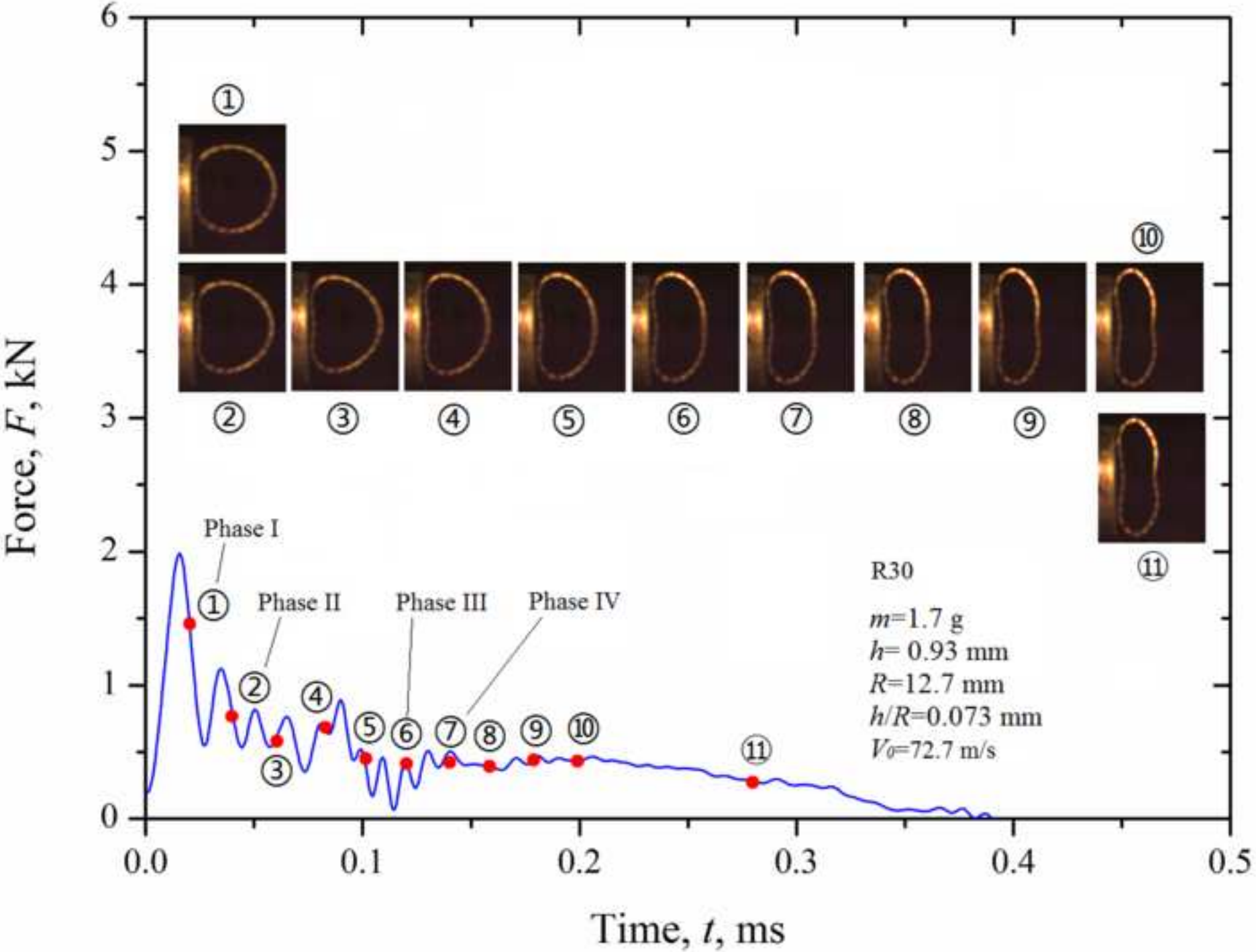

Table 1

Table 1. Summary of ring collision tests

Specimen	Mass (g)	Outer Diameter (mm)	Wall Thickness (mm)	Ring Width (mm)	Initial Velocity (m/s)	Rebounding Velocity (m/s)
R1	1.8	28.55	0.9	9.16	17.7	7.8
R2	1.8	28.51	0.9	9.15	23.8	9.9
R3	1.9	28.63	0.87	9.15	48.3	13.5
R4	1.9	28.56	0.92	9.1	49.0	13.7
R5	1.9	28.54	0.92	9.07	54.7	14.2
R6	1.9	28.52	0.91	9.14	56.5	14.0
R7	1.9	28.5	0.92	9.07	59.4	13.4
R8	1.9	28.5	0.91	9.15	68.7	13.2
R9	1.9	28.52	0.9	9.05	71.7	11.8
R10	1.9	28.58	0.89	9.13	78.2	9.5
R11	1.9	28.52	0.91	9.15	83.3	8.6
R12	1.9	28.52	0.91	9.14	87.1	9.1
R13	1.9	28.55	0.9	9	94.4	3.7
R14	1.9	28.5	0.9	9.14	97.7	3.8
R15	1.9	28.51	0.89	9.08	100.0	4.2
R16	1.9	28.55	0.9	9.09	110.2	7.3
R17	1.9	28.47	0.9	9.15	125.0	6.9
R18	1.7	25.42	0.92	9.11	16.5	7.5
R19	1.7	25.4	0.91	9.04	19.8	8.7
R20	1.7	25.4	0.92	9.08	31.2	11.0
R21	1.7	25.42	0.92	9.12	33.7	12.7
R22	1.7	25.4	0.9	9.08	40.4	13.5
R23	1.7	25.43	0.92	9.08	41.3	14.1
R24	1.7	25.42	0.93	9.07	42.1	13.9
R25	1.7	25.42	0.92	9.1	59.0	13.3
R26	1.7	25.4	0.92	9.05	60.0	13.7
R27	1.7	25.43	0.92	9.1	61.2	13.6
R28	1.7	25.42	0.91	9.05	61.2	13.4
R29	1.7	25.39	0.92	9.11	63.6	14.3
R30	1.7	25.41	0.93	9.1	72.7	12.2
R31	1.7	25.4	0.92	9.07	79.9	10.3
R32	1.7	25.4	0.92	9.1	81.1	10.2
R33	1.6	25.43	0.92	9.11	81.6	10.2
R34	1.7	25.4	0.93	9.11	84.2	9.5
R35	1.7	25.39	0.91	9.07	93.5	7.3
R36	1.7	25.42	0.93	9.05	101.4	4.1
R37	2.4	25.39	1.29	9.11	17.2	8.4
R38	2.3	25.41	1.29	9.24	39.5	12.5
R39	2.3	25.41	1.29	9.24	43.5	14.1
R40	2.4	25.4	1.28	9.19	52.5	13.7
R41	2.4	25.41	1.28	9.14	60.1	14.8

R42	2.3	25.43	1.28	8.94	66.3	14.9
R43	2.3	25.4	1.28	9.08	76.5	12.7
R44	2.3	25.39	1.29	9.18	78.1	12.7
R45	2.3	25.44	1.28	9.1	91.8	10.5
R46	2.3	25.4	1.29	9.19	114.8	7.0